Available online at www.sciencedirect.com
SCIENCE DIRECT®
PERGAMON
Applied Geochemistry 18 (2003) 1225–1239
Applied Geochemistry
www.elsevier.com/locate/apgeochem

Kinetic dissolution of carbonates and Mn oxides in acidic water: measurement of in situ field rates and reactive transport modeling

James G. Brown[a,*], Pierre D. Glynn[b]

[a]US Geological Survey, Tucson, AZ 85719, USA
[b]US Geological Survey, National Center, Reston, VA 20192, USA

Received 7 February 2002; accepted 3 January 2003
Editorial handling by R.L. Bassett

Abstract

The kinetics of carbonate and Mn oxide dissolution under acidic conditions were examined through the in situ exposure of pure phase samples to acidic ground water in Pinal Creek Basin, Arizona. The average long-term calculated in situ dissolution rates for calcite and dolomite were 1.65×10^{-7} and 3.64×10^{-10} mmol/(cm^2 s), respectively, which were about 3 orders of magnitude slower than rates derived in laboratory experiments by other investigators. Application of both in situ and lab-derived calcite and dolomite dissolution rates to equilibrium reactive transport simulations of a column experiment did not improve the fit to measured outflow chemistry: at the spatial and temporal scales of the column experiment, the use of an equilibrium model adequately simulated carbonate dissolution in the column. Pyrolusite (MnO_2) exposed to acidic ground water for 595 days increased slightly in weight despite thermodynamic conditions that favored dissolution. This result might be related to a recent finding by another investigator that the reductive dissolution of pyrolusite is accompanied by the precipitation of a mixed Mn–Fe oxide species. In PHREEQC reactive transport simulations, the incorporation of Mn kinetics improved the fit between observed and simulated behavior at the column and field scales, although the column-fitted rate for Mn-oxide dissolution was about 4 orders of magnitude greater than the field-fitted rate. Remaining differences between observed and simulated contaminant transport trends at the Pinal Creek site were likely related to factors other than the Mn oxide dissolution rate, such as the concentration of Fe oxide surface sites available for adsorption, the effects of competition among dissolved species for available surface sites, or reactions not included in the model.
Published by Elsevier Science Ltd.

1. Introduction

At many field sites, geochemical reactions that control the fate and transport of contaminants in ground water or surface water cannot be characterized adequately by equilibrium processes alone. In many instances, knowledge of the rates at which selected reactions occur is necessary to understand important processes and to develop effective remediation plans. Laboratory-derived rates are sometimes the only source of information on reaction kinetics; unfortunately, such rates typically differ significantly from field reaction rates. This paper presents the results of an in situ study of field dissolution rates of calcite, dolomite, and Mn oxides, and applies the field- and laboratory-derived rates to reactive transport simulations at column and field scales. The simulations discussed in this paper were done using either version one or version two of the PHREEQC geochemical computer code (Parkhurst, 1995; Parkhurst and Appelo, 1999). Only version two has the capability to simulate kinetic reactive transport.

* Corresponding author. Tel.: +1-520-670-6671.
E-mail address: jgbrown@usgs.gov (J.G. Brown).

0883-2927/03/$ - see front matter Published by Elsevier Science Ltd.
doi:10.1016/S0883-2927(03)00010-6

1.1. Description of site and contaminant plume

Pinal Creek Basin, located about 100 km east of the Phoenix metropolitan area (Fig. 1), has been an area of large-scale Cu mining since the late 1800s. Multiple contaminant sources, including seepage of acidic mine-process water from unlined impoundments into underlying unconsolidated alluvium, have resulted in a 25-km-long plume of acidic ground water in the principal aquifer of the basin. The aquifer consists of two units, the oldest of which is a semiconsolidated to consolidated basin fill that consists mainly of sand, gravel, and conglomerate but locally includes fine-grained lakebed deposits (Neaville and Brown, 1994) Unconsolidated stream alluvium underlies the major drainages and is incised into the underlying basin fill. The stream alluvium, which consists mainly of sand and gravel, is from 300 to 800 m wide and has a maximum thickness of about 50 m.

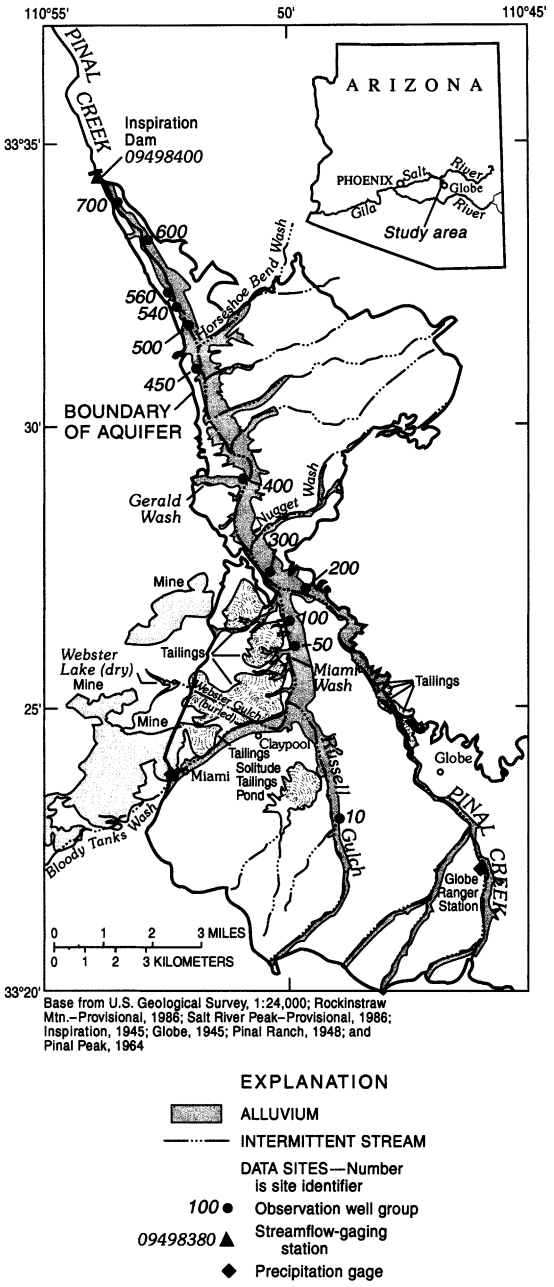

Fig. 1. Pinal Creek Basin, Arizona.

The plume consists of 3 distinct hydro-chemical zones, each characterized by a unique aqueous and solid-phase chemistry (Fig. 2). From 1984 to 1999, the pH of the most acidic part of the plume remained near 4, and the concentrations of most other constituents decreased significantly. From 1984 to 1999 concentrations of dissolved SO_4 in water from well 51 decreased from about 100 mmol/l (Table 1) to 30 mmol/l, and concentrations of dissolved Fe decreased from 57 to 3 mmol/l. Concentrations of dissolved Cu decreased from 2 to 1 mmol/l, and concentrations of dissolved Al decreased from 11 to 2.4 mmol/L. In the transition zone, the reductive dissolution of Mn oxide coupled to the oxidation of Fe^{2+} and precipitation of Fe hydroxide generates protons and contributes additional acidity to the ground water. The dissolution of carbonate minerals and, to a lesser extent silicate minerals, consumes protons. The net result of these reactions is to raise the pH to more than 5, which increases the pH-dependant adsorption of metals such as Cu, Co, Ni, and Zn. In the neutralized zone Ca and SO_4 are the dominant ions, and trace metals generally occur near or below laboratory minimum reporting levels. In 1998, the concentration of dissolved Mn decreased down-gradient in the neutralized zone from more than 50 mg/l to about 1 mg/l, probably through the precipitation of Mn carbonate (rhodochrosite) (Brown et al., 1998). Eychaner (1991) estimated that the transition zone of the plume migrated down-valley over the previous several decades at a velocity of 0.2–0.3 km/a. In contrast, ground water was estimated to flow at a rate of 5 m/d, or about 1.8 km/a (Brown et al., 1998), about 7 times faster.

1.2. Previous work at site

Current USGS studies at Pinal Creek began in 1984. Since then, the movement and transformation of contaminants has been characterized by a combination of field, laboratory, and model investigations (Brown and Favor, 1996; Glynn and Brown, 1996; Morganwalp and Buxton, 1999). Stollenwerk (1994) characterized and modeled the evolution of the contaminant plume through 1987, and Brown et al. (1998, 2000) applied 1-dimensional equilibrium models to the evolution of the plume from 1984 through 1994 using the geochemical model PHREEQC (Parkhurst and Appelo, 1999). Glynn

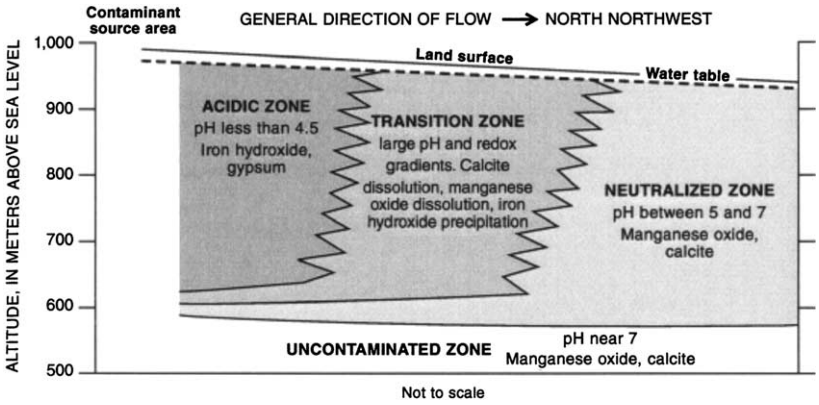

Fig. 2. Generalized longitudinal section indicating hydrochemical zones in the aquifer.

and Brown (1996) investigated the sensitivity of transport rates of low-pH reducing water to postulated reactions thought to occur at the site. Brown et al., (1998, 2000) noted the lack of local equilibrium for selected reactions and suggested the need for a kinetic approach to better model the evolution of the plume at the site.

2. In situ experimental methods

For the in situ experiment, calcite ($CaCO_3$), dolomite ($CaMg(CO_3)_2$), and pyrolusite (MnO_2) were exposed to acidic ground water in project monitor wells for periods ranging from 16 to 595 days beginning in April 1998 (Table 2). Preliminary in situ experiments by Lind et al. (1998) determined suitable mesh sizes and material with which to suspend sediments. Tests done using 21- and 67-μm filters indicated that the rates of reaction between in situ materials and ground-water were not affected by filter size. On the basis of these findings, calcite and dolomite particles that ranged from 75 to 150 μm in diameter (the size of fine sand) were used with 21-μm polyester macroporous filters (PEMF) in this experiment. Subsequent to the experiment using sized material, possible effects of mesh size on the measured rates were examined in a second experiment in which 21- and 800-μm diameter meshes were used to enclose single calcite crystals, which were then exposed to acidic ground water for 180 days.

2.1. Preparation of samples and placement in wells

Pure-phase samples of Iceland-spar calcite, dolomite, and pyrolusite were obtained commercially. For the first experiment, crystals of each mineral were ground using a mortar and pestle and sorted using non-metallic sieves. Scanning electron microscope analysis of the carbonates indicated that the calcite contained as much as 0.1 wt.% FeO and 0.15–0.3 wt.% Mg. The dolomite contained as much as 0.96 wt.% FeO and 0.3–0.9 wt.% Mn. The sized samples were then gently rinsed to remove any smaller-sized particles that may have adhered to the 75–150-μm-diameter particles. The samples were oven dried, then placed and weighed on flat 5 by 5 cm squares of PEMF mesh, which were then fashioned into sacks and tied at the top with nylon monofilament line. The sized Mn oxide could not be placed in the PEMF sack without loss of material because static electricity caused the Mn oxide to spread out beyond the center of the mesh. To circumvent this problem, a mesh was used to line a support structure fashioned from a 30-ml polypropylene jar from which 3 sections were removed from the vertical sides. The combined weight of the sample and container were then measured prior to placement in the well. Manganese weight loss was determined from the difference of the total weight of the material, mesh, and support structure before and after exposure to the acidic water.

For the single crystal experiment, each calcite crystal was washed and dried in a manner similar to that of the sized materials, and weighed. One crystal was enclosed in a sack fashioned from the 75-μm diameter mesh; another was placed in a support structure fitted with a cylindrically shaped rectangular piece of 800-μm diameter mesh.

The carbonate and pyrolusite sample containers were attached to the end of 2.5-cm diameter polyvinyl chloride (pvc) pipe and suspended at the middle of the screen of wells 304 and 101. Sized calcite samples were suspended for periods ranging from 14 to 265 days beginning in April 1998. Single calcite samples were suspended for 180 days beginning May 2001. Dolomite samples were exposed for periods ranging from 96 to 595 days (Table 2). The pyrolusite samples were exposed for periods ranging from 240 to 570 days beginning in May 1998.

Table 1
Measured water chemistry of wells and surface water, Pinal Creek Basin, AZ, 1984–1993[a]

Site	Date	Temp. (°C)	pH	Ca	Mg	Na	K	C	SO_4	Cl	Si	Fe	Mn	Al	Cu	Co	Ni	Sr	Zn
51	November 1984	18.0	3.7	12.2	16.0	10.0	0.24	4.08	104.	10.2	1.66	57.3	1.33	11.1	2.36	0.18	0.065	0.017	0.29
101	November 1984	18.0	3.6	11.5	12.3	8.26	0.25	4.42	73.9	10.4	1.65	39.4	1.04	8.54	1.89	0.14	0.054	0.018	0.18
202	March 1985	13.5	7.2	1.2	0.37	0.96	0.036	–	0.70	0.48	0.36	0.0007	<0.0006	0.003	0.0002	<0.0003	<0.0085	0.0023	<0.0002
302	November 1984	–	3.5	16.7	11.9	6.96	0.21	4.91	71.8	8.74	1.83	32.2	1.09	6.69	1.53	0.12	0.051	0.034	0.14
402	November 1984	18.0	4.1	13.0	5.76	3.48	0.19	4.08	27.1	3.95	1.45	6.27	0.91	0.409	0.30	0.030	0.019	0.020	0.046
451	March 1989	19.0	4.9	14.7	5.47	3.59	0.28	4.67	24.8	5.13	1.14	2.47	1.89	0.153	0.18	0.031	0.020	0.018	0.53
503	July 1986	17.5	6.2	15.2	5.76	3.39	0.11	–	20.8	3.67	1.01	0.0032	0.82	0.0007	0.0005	<0.0002	0.007	0.240	0.0029
702	May 1990	20.0	7.0	13.7	5.06	3.03	0.16	–	18.2	2.34	0.46	0.019	0.052	0.186	0.002	<0.003	<0.008	0.027	0.002
PCID	January 1993	14.0	7.7	1.4	0.31	0.33	0.087	–	1.46	0.107	–	0.0001	0.001	–	0.0002	–	–	–	<0.00005

[a] Values are in millimoles/l unless otherwise indicated, expect for temperature which is in degrees celsius, and pH. Dashes indicate no data; <, less than; PCID, Pinal Creek at Inspiration Dam.

During the experiment using the sized carbonates, the measured pH of water from well 304 decreased from 4.1 to 4.0, and the concentrations of most constituents increased (Table 3). For example, dissolved Fe increased from 2.23 mmol/l in June 1998 to 2.71 mmol/l in December 1999, and dissolved Cu increased from 0.17 to 0.28 mmol/l. The water was undersaturated with respect to calcite and dolomite for the entire experiment. The saturation index (SI) values calculated using the PHREEQC code varied from −5.32 to −5.44 for calcite and from −11.0 to 11.2 for dolomite. SI values for both minerals showed only a slight trend away from equilibirium over time.

During the experiment using the single calcite crystals, the measured pH of water from well 304 was 4.0, and the concentrations of most constituents decreased (Table 3). Dissolved Fe decreased from 2.01 mmol/l in May 2001 to 1.81 mmol/l in May 2002 and dissolved Cu increased from 0.17 to 0.28 mmol/l. The water was under-saturated with respect to calcite and dolomite for the entire experiment. Calculated SI values for calcite and dolomite were similar to those calculated for the sized-carbonate experiment.

From June 1998 to December 1999 the pH of water from well 101 decreased from 4.1 to 3.9, and the concentration of dissolved Fe more than doubled from 2.50 to 6.40 mmol/l. Other concentrations increased as well: dissolved Mn increased from 0.16 to 0.50 mmol/l, and dissolved Cu increased from 0.19 to 0.64 mmoI/l. Calculated pyrolusite SI values increased from −19.9 to −15.5.

2.2. Post-exposure sample analysis

To remove each sample, the support pipe was removed from the well and the sample cluster was quickly placed in a N_2-filled glove bag. This minimized but did not eliminate exposure to the atmosphere after removal from the well and before drying. The appropriate PEMF mesh sack was cut off from the coupling and placed in a N_2-flushed bottle or zip-lock bag for further processing. Samples were rinsed gently with deionized water either immediately upon removal from the well, or upon removal from the bottle or zip-lock bag in the laboratory. The sample-filled PEMF sacks were dried for at least 4.5 h at 100–110 °C, and then weighed. The minerals were then removed from the PEMF sack, which was rinsed, dried, and reweighed. The sized carbonate material was not weighed directly because of the difficulty in removing the samples from the mesh sacks without losing small amounts of material. The sample weight was calculated by subtracting the weight of the PEMF mesh from the weight of the sample-filled PEMF sack.

The measured decreases in carbonate mass ranged from 0.0534 to 0.4527 g, or from 5 to 44% of the initial

Table 2
Exposure times and calculated in situ mineral dissolution rates

Sample	Exposure time (days)	Initial weight (g)	Final weight (g)	Weight change (g)	Pct. weight change	Initial surface area (cm^2)	Dissolution rate (mmol/(cm^2 s))
Calcite, 75–150 μm	14	1.0124	0.9590	−0.0534	−5.27	209	2.15×10^{-9}
Calcite, 75–150 μm	40	1.0197	0.8248	−0.1949	−19.1	211	2.87×10^{-9}
Calcite, 75–150 μm	96	1.0216	0.8511	−0.1705	−16.7	211	1.03×10^{-9}
Calcite, 75–150 μm	169	1.0936	0.7704	−0.3232	−29.6	226	1.09×10^{-9}
Calcite, 75–150 μm	265	1.0211	0.5684	−0.4527	−44.3	211	1.11×10^{-9}
Calcite, single crystal, 21-μm mesh	180	19.8983	19.8152	−0.0831	−0.418	22.5	2.38×10^{-9}
Calcite, single crystal, 800-μm mesh	180	19.8965	19.6776	−0.2189	−1.100	28.5	4.97×10^{-9}
Dolomite, 75–150 μm	96	0.8003	0.6878	−0.1125	−14.1	157	4.92×10^{-10}
Dolomite, 75–150 μm	265	0.7816	0.5882	−0.1934	−24.7	154	3.27×10^{-10}
Dolomite, 75–150 μm	595	0.7336	0.4161	−0.3175	−43.3	144	2.74×10^{-10}
Pyrolusite, 75–150 μm	240	1.0743	1.1054	+0.0311	+2.89	–	–
Pyrolusite, 75–150 μm	570	1.3114	1.3512	+0.0398	+3.03	–	–

weights of the sample-filled sacks (Table 2). Calibration checks of the balance were made before and after each weighing session using National Bureau of Standards Class P weights. These checks, and repeated weighings of bagged carbonates, agreed to within 0.0006 g, about 1% of the minimum measured decrease. If additive, these sources of uncertainty could contribute to a 2% error in the measured decreases in mineral mass.

Microphotographs of the sized calcite and dolomite samples indicated that particle shapes ranged from rhombohedral to irregular. For the purpose of estimating the total surface area of each sample, a rhombohedral shape was assumed. The average measured ratios of the length of the 3 sides of 2 rhombohedral calcite crystals were 0.735:1:3:1 (C.J. Lind, USGS, personal communication, 1998). Using a mean length of 112 μm for the middle dimension, the initial surface areas of the calcite and dolomite samples were calculated to be 207 and 196 cm^2/g, respectively.

After 14 days of exposure, all the calcite samples were stained orange by Fe hydroxide precipitation. Microscopic examination of calcite grains in thin section indicated that staining increased with time from 14 to 169 days, but that the sample retrieved after 265 days was tinted to the same degree as the 169-day sample (Owen Bricker, US Geological Survey, personal communication, 2000). The dolomite sacks were only slightly tinted. Microscopic, thin-section examination indicated that staining of dolomite grains was virtually nonexistent.

3. In situ experiment results and discussion

For the carbonate samples, the dissolution rate for each sample was calculated on the basis of the measured decrease in weight, exposure time, and estimated surface area. The measured decreases in calcite mass ranged from 0.0534 g after 14 days of exposure to 0.4527 g after 265 days of exposure. The measured decreases in dolomite mass ranged from 0.1125 g after 96 days to 0.3175 g after 595 days (Table 2). The ratio of the final weight to the initial weight of calcite and dolomite samples decreased linearly with time, with the exception of sample C2. Sample weights used for the determination of surface areas were the average of the initial and final weights for each sample. Surface area/weight ratios were calculated for each sample to account for measured decreases in mass that occurred over each exposure period.

3.1. Calcite in situ dissolution rates

For the single crystals, calculated dissolution rates were 4.97×10^{-9} mmol/(cm^2 s) for the 800 μm mesh and 2.38×10^{-9} mmol/(cm^2 s) for the 21 μm mesh after 180 days (Table 2, Fig. 3). For the sized calcite in 21 μm

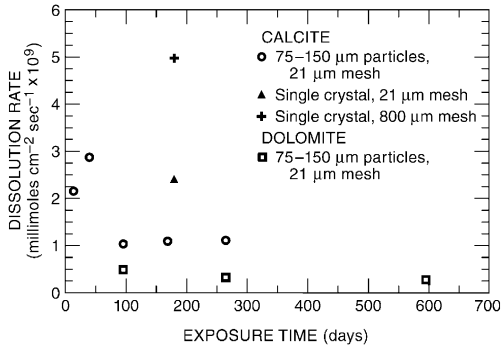

Fig. 3. Calcite and dolomite in situ dissolution rates.

Table 3
Water chemistry of wells 304 and 101 during in situ experiment, 1998–2002

Well	Date	Temp. (°C)	pH	Ca	Mg	Na	K	C	SO_4	Cl	Si	Fe	Mn	Al	Cu	Co	Ni	Sr	Zn	$SI_{Calcite}$	$SI_{dolomite}$	$SI_{pyrolusite}$
304	June 1998	21.0	4.1	5.77	2.32	2.47	0.11	3.17	12.3	1.76	1.30	2.23	0.20	0.52	0.17	–	0.005	0.011	0.027	−5.32	−11.0	−13.9
304	December 1999	17.0	4.0	8.48	3.54	3.27	0.13	2.83	18.1	2.12	1.45	2.71	0.31	0.83	0.28	0.01	0.008	0.016	0.036	−5.44	−11.2	−14.6
304	May 2001	20.5	4.0	6.64	2.82	2.48	0.14	3.00	13.2	1.53	1.28	2.01	0.25	0.69	0.24	0.01	0.006	0.012	0.034	−5.44	−11.2	−14.2
304	May 2002	20.5	4.0	8.41	3.59	2.99	0.13	2.35	17.3	2.35	1.36	1.81	0.34	1.02	0.31	0.01	0.008	0.015	0.037	−5.42	−11.1	−14.1
101	June 1998	21.5	4.1	3.82	2.04	2.60	0.15	3.75	10.6	1.54	1.27	2.50	0.16	0.51	0.19	–	0.004	0.011	0.027	−5.42	−11.0	−19.9
101	December 1999	14.0	3.9	10.63	6.21	3.76	0.23	3.83	29.6	1.57	1.37	6.40	0.50	2.06	0.64	0.03	0.015	0.025	0.079	−5.63	−11.5	−15.5

Values are in millimoles/l except for temperature, pH, and the saturation index. Dashes indicate no data; water filtered through 0.45 μm filter prior to analysis (except for pH).

mesh, the measured calcite dissolution rates ranged from 2.87×10^{-9} mmol/(cm^2 s) after 40 days of exposure to 1.03×10^{-9} mmol/(cm^2 s) after 96 days (Table 2, Fig. 3), and increased slightly to 1.11×10^{-9} mmol/(cm^2 s) after 265 days. The mean rate from the 5 sized samples was 1.65×10^{-9} mmol/(cm^2 s) (Table 4).

The use of the 21 μm mesh decreased the initial rates by a factor of two on the basis of a comparison of the single crystal rates after 180 days with the rates measured on the sized calcite made after 14 and 40 days of exposure. The decrease to a calculated rate of 1.03×10^{-9} mmol/(cm^2 s) is more likely related to the precipitation of iron on the sized calcite than to the rate of flow through the 21 μm mesh. Similarly, the early time rates for the sized calcite of more than 2×10^{-9} mmol/(cm^2 s) indicate that the slower measured dolomite rates were not limited by flow through the 21 μm mesh.

Regardless of the mesh size used, these rates were significantly slower than laboratory rates measured by Plummer et al. (1978). In their experiments, Plummer et al. (1978) dissolved calcite by adding HCl to a stirred beaker containing Iceland spar in deionized water at a fixed pCO_2, over a pH range from 2 to 7 and a temperature range from 0 to 60 °C. They found that calcite dissolution could be described by an equation of the form,

$$R = k_1[H^+] + k_2[H_2CO_3^*] + k_3[H_2O] - k_4[Ca^{++}][HCO_3^-] \quad (1)$$

where R is the dissolution rate in mmol/(cm^2 s), k_1, k_2, and k_3, are the forward rate constants in cm/s (each a function of temperature), k_4 is the backward rate constant (a function of temperature and P_{CO_2}), H_2CO_3* represents the sum of the $CO_{2(aq)} + H_2CO_3^0$ species, and brackets denote the activity (unitless) of the indicated constituent. At a pH of 4.0–4.1, which was the pH associated with the situ experiment, the fourth term of Eq. (1) is insignificant. Applying Eq. (1) to the average chemical conditions for the in situ experiment, and using the rate constants derived by Plummer et al. (1978) for their laboratory experiments, resulted in a rate of 3.98×10^{-6} mmol/(cm^2 s) (Table 4). This rate is more than 3 orders of magnitude higher than the field rate calculated in the present study. Plummer et al. (1978) also found that at a pH of 4, decreasing the stirring rate by a factor of about 3 caused the measured dissolution rate to decrease by a factor of about 2. This decrease was small given the differences between the laboratory rates determined by Plummer et al. (1978) and the field rates estimated from the in situ experiments.

3.2. Dolomite in situ dissolution rates

The dolomite in situ dissolution rate decreased from 4.92×10^{-10} mmol/(cm^2 s) after 96 days to 2.74×10^{-10}

Table 4
Estimated carbonate dissolution rates under conditions of in situ experiment

Mineral	Source of dissolution rate	Rate (mmol/(cm^2 s))
Calcite	In situ experiment[a]	1.65×10^{-9}
Calcite	Plummer et al. (1978) lab rate[b]	3.98×10^{-6}
Dolomite	In situ experiment[c]	3.64×10^{-10}
Dolomite	Busenberg and Plummer (1982) lab rate[b]	3.04×10^{-7}

[a] Mean rate from 5 samples.
[b] Calculated using well 304 average water chemistry during in situ experiment.
[c] Mean rate from 3 samples.

mmol/(cm^2 s) after 595 days (Fig. 3). The mean of the 3 measurements was 3.64×10^{-10} mmol/(cm^2 s) (Table 4). Unfortunately, a dolomite sample was not collected after 14 days; therefore, the dolomite rate during the first weeks of exposure is unknown. The lack of any orange staining on the dolomite, however, suggests that decreases in dissolution rates through time caused by coating of the mineral grains by Fe precipitation would be minimal for dolomite. Busenberg and Plummer (1982) noted that upon exposure to acidic conditions the $CaCO_3$ component in dolomite dissolved preferentially relative to $MgCO_3$, so that the higher initial dolomite dissolution rates may have beeen related to this initial preferential Ca dissolution.

In the laboratory, Busenberg and Plummer (1982) found that the net dolomite dissolution rate R could be described by the equation:

$$R = k_1\left[H^+\right]^n + k_2\left[H_2CO_3^*\right]^n + k_3[H_2O]^n - k_4\left[HCO_3^-\right] \quad (2)$$

where k_1, k_2, k_3 are forward rate constants in (mmol kg_{water})$^{1/2}$/(cm^2 s $10^{1.5}$) (approximately (mol/cm)$^{1/2}$/s in dilute solutions), k_4 is the backward rate constant in cm/s (in dilute solutions), and n equals 0.5 at temperatures at or below 45 °C. For the average ground-water chemistry during the in situ experiment, the backwards rate is insignificant, and the rate can be expressed using only the first 3 terms. For the average water chemistry during the in situ experiment, R was calculated to be 3.04×10^{-7} mmol/(cm^2 s) (Table 4). As was the case for calcite dissolution, the in situ field rate was about 3 orders of magnitude less than the rate calculated from the laboratory-derived rate equation.

3.3. Mn oxide in situ dissolution rates

Manganese oxide samples were exposed to acidic water in well 101 for 240 and 570 days. Over this period the weights of the Mn oxide samples increased slightly during the in situ experiment, contrary to expectations. The apparent lack of dissolution is incompatible with (1) the estimated decrease in Mn oxide concentration that occurred in the column experiment of Stollenwerk (1994) and (2) saturation indices that ranged from −19.9 to −15.5, which indicated that thermodynamic conditions in well 101 favored pyrolusite dissolution. In a study of Mn oxide dissolution in a flow-through reaction cell, Villinski et al. (2001) found using X-ray spectroscopy that the dissolution of MnO_2 was accompanied by the precipitation of a phase with the structure of jacobsite ($MnFe_2O_4$). The formation of this phase could at least partially explain the apparent formation of Mn oxide during the in situ experiment. Another reason might be related to the actual Mn oxide phase present in the aquifer. The Mn oxide phase initially in the aquifer has not been determined, and the use of birnessite or some other Mn oxide mineral, rather than pyrolusite, might have produced different results. Future experiments done using alternative phases might provide useful information on the relative rates at which birnessite, pyrolusite, or other Mn oxide phases reductively dissolve in the aquifer.

4. Kinetic modeling of mineral dissolution at the column scale

As mentioned previously, geochemical transport simulations of plume evolution and column experiments of acidic breakthrough indicated that the local equilibrium assumption was not met for selected reactions. This lack of equilibrium was most evident for Mn oxide minerals (Brown et al., 1998, 2000), although the possibility of kinetically slow carbonate dissolution reactions also was noted (Brown et al., 1998).

In an effort to examine the applicability of laboratory- and field-derived rate estimates to column-scale reactive transport, reaction kinetics for calcite and Mn oxide dissolution were incorporated in numerical simulations of Stollenwerk's column experiment (Stollenwerk, 1994). In the column experiment, almost 11 pore volumes of acidic ground water from Pinal Creek Basin were eluted through a 0.8-m-long column of uncontaminated Pinal Creek alluvium (Table 5). The velocity of flow through the column was 0.4 m/d, about 1 order of magnitude less than the average linear velocity of 5 m/d estimated for the alluvium. The simulated column was divided into 10 cells of equal length. Each shift of water and solutes from one cell to the next represented 0.2 days, or 1/10th of a pore-volume. The measured and simulated breakthrough of Cl, a conservative constituent in the ground-water system at Pinal Creek, occurred at pore volume 1. The measured breakthrough of acid water occurred at about pore volume 3 (Figs. 4 and 5). The retardation of acidic breakthrough relative to that of Cl, a conservative constituent, was controlled mainly by the dissolution of calcite and the reductive

Table 5
Water chemistry for column simulations[a]

Constituent	Initial chemistry in column	Chemistry of acidic inflow
pH	8.20	3.30
Calcium	1.2	11.6
Magnesium	0.37	15.8
Sodium	0.96	9.4
Potassium	0.03	0.2
Total carbon	2.3	4.08
Sulfate	0.7	100
Chloride	0.48	9.5
Fluoride	0.0158	1.6
Silica	0.40	1.86
Iron	0.00035	52.4
Manganese	0.0001	1.34
Aluminum	0.018	10.5
Cadmium	0.0000045	0.0052
Copper	0.00015	2.4
Cobalt	0.0005	0.2
Nickel	0.001	0.06
Strontium	0.0027	0.015
Zinc	0.00025	0.33

[a] Values in millimoles/l, except for pH.

dissolution of Mn oxide, which was was coupled to the oxidation and precipitation of Fe hydroxide. The breakthroughs of trace elements such as Cu, Co, Ni, and Zn, were determined to be controlled by pH-dependent adsorption and desorption from Fe hydroxide surfaces (Stollenwerk, 1994) At about pore volume 11, column inflow was switched to uncontaminated water. Outflow pH remained less than 4.5 through pore volume 20, mainly as a result of the desorption of protons from Fe hydroxide.

In an equilibrium model (Brown et al., 2000) of the column experiment, the concentration of selected dissolved constituents was controlled by equilibrium with calcite, dolomite, gypsum ($CaSO_4$), ferrihydrite [$Fe(OH)_{3(a)}$], Mn oxide, and amorphous silica ($SiO_{2(a)}$) (Table 6); and adsorption and desorption from Fe hydroxide surfaces (Table 7). The present analysis focused on the effects of Mn oxide and carbonate dissolution kinetics on the acidic breakthrough in the column and on the magnitude of the Mn breakthrough peak in the column outflow. Two significant changes were made to the Brown et al. (2000) equilibrium simulation. The number of surface complexation sites was increased from 5 to 20% of the values of 0.005 mol per mol $Fe(OH)_{3(a)}$ for strong (type 1) sites and 0.2 mol per mol $Fe(OH)_{3(a)}$ for weak (type 2) sites used for hydrous Fe(III) oxide (HFO) by Dzombak and Morel (1990). This brought the number of simulated complexation sites to within the experimental range of site densities found by Dzombak and Morel (1990) in their review and compilation of available data. Secondly, for comparison with the calcite kinetic dissolution models, dolomite was removed from the equilibrium model, leaving calcite as the only carbonate mineral available for dissolution. Details on other aspects of the simulation are discussed by Brown et al. (2000). For clarity, the simulations discussed in this paper are referred to by descriptive abbreviations (Tables 8 and 9).

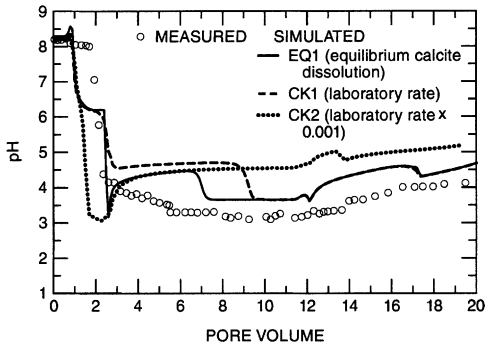

Fig. 4. Measured and simulated pH in column effluent showing effects of equilibrium and kinetic calcite dissolution.

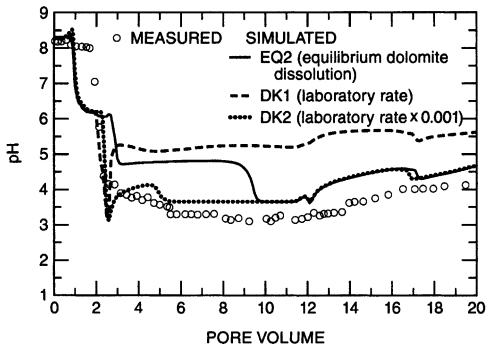

Fig. 5. Measured and simulated pH in column effluent showing effect of equilibrium and kinetic dolomite dissolution. Laboratory rate from Busenberg and Plummer (1982). Column simulations parameters are summarized in Tables 5–8.

Table 6
Mineral equilibria and the logarithms of solubility-product constants used in column and field simulations

Mineral	Reaction	LogK_{sp}
Calcite	$CaCO_{3(c)} = Ca^{2+} + CO_3^{2-}$	−8.48
Dolomite[a]	$Ca,Mg(CO_3)_2 = Ca^{+2} + Mg^{+2} + 2CO_3^{-2}$	−16.54
Gypsum	$CaSO_{4(c)}.(2H_2O) = Ca^{2+} + SO_4^{2-} + 2H_2O$	−4.58
Ferrihydrite	$Fe(OH)_{3(a)} + 3H^+ = Fe^{3+} + 3H_2O$	4.89
Mn oxide	$MnO_{2(c)} + 4H^+ + 2e^- = Mn^{2+} + 2H_2O$	41.38
Rhodochrosite[a]	$MnCO_{3(c)} = Mn^{2+} + CO_3^{2-}$	−11.13
Silica[b]	$SiO_{2(a)} + 2H_2O = H_4SiO_4$	−2.71

Source: PHREEQC database (Parkhurst and Appelo, 1999).
[a] Accounted for in field simulation only.
[b] Accounted for in column simulation only.

Table 7
Surface reactions and equilibrium constants used in column and field simulations. Surf_OH is the uncharged surface complexation site

Adsorption reaction	Log*K* weak sites	Log*K* strong sites
$Surf\_OH = Surf\_OH$	0.0	0.0
$Surf\_OH + H^+ = Surf\_OH_2^+$	7.29	7.29
$Surf\_OH = Surf\_O^- + H^+$	−8.93	−8.93
$Surf\_OH + Ca^{+2} = Surf\_OCa^+ + H^+$	−5.85	–
$Surf\_OH + Ca^{+2} = Surf\_OHCa^{+2}$	–[a]	4.97
$Surf\_OH + H^+ + SO_4^{-2} = Surf\_SO_4^- + H_2O$	7.78	–
$Surf\_OH + SO_4^{-2} = Surf\_OHSO_4^{-2}$	0.79	–
$Surf\_OH + Cu^{+2} = Surf\_OCu^+ + H^+$	0.6	2.89
$Surf\_OH + Co^{+2} = Surf\_OCo^+ + H^+$	−3.01	−0.46
$Surf\_OH + Ni^{+2} = Surf\_ONi^+ + H^+$	−2.5	0.37
$Surf\_OH + Zn^{+2} = Surf\_OZn^+ + H^+$	−1.99	0.99
$Surf\_OH + Mn^{+2} = Surf\_OMn^+ + H^+$	−3.5	–
$Surf\_OH + Mn^{+2} = Surf\_OHMn^{+2}$	–	−0.4
$Surf\_OH + Mg^{+2} = Surf\_OMg^+ + H^+$	−4.6	4.9[b]

Source unless otherwise noted: Dzombak and Morel (1990).
[a] Dashes indicate *K* not available for indicated site.
[b] Estimated from thermodynamic data-field simulation only.

4.1. Calcite

The rate expression of Plummer et al. [1978; Eq. (1)] for calcite dissolution and precipitation was added to the modified equilibrium simulation of Brown et al. (2000). For use in PHREEQC, the forward rate was given by

$$r_f = k_1[H^+] + k_2[H_2CO_3^*] + k_3[H_2O] \quad (3)$$

and the overall rate was approximated by

$$R = r_f\left[1 - \left(\frac{IAP}{K_{calcite}}\right)^{2/3}\right] \quad (4)$$

where r_f is the forward rate, IAP is the ion activity product for calcite, and $K_{calcite}$ is the solubility product constant for calcite. In the kinetic model, the overall rate was multiplied by a parameter (referred to in the PHREEQC code as PARM1) that accounts for the reactive calcite surface area per cell. A PARM1 value of 1393 was calculated from the initial calcite content of 0.067 mol/l_{water} in the column and from the surface-area-to-weight ratio estimated for the in situ experiment material. Because the carbonate surfaces in the natural alluvium are likely to be much more irregular than those of the sized material used in the in situ experiment and are probably often present as coatings or cements rather than as single crystals, this PARM1 value likely represents a minimum estimate of the surface area of calcite in the column.

Two simulations were done using different calcite dissolution rates. The first, referred to as CK1, used the rate equation and laboratory-derived rate constants of Plummer et al. (1978). For the second kinetic simulation (CK2), the rate of Plummer et al. (1978) was multiplied by 10^{-3} to approximate the calcite dissolution rate calculated from the in situ experiments.

For the equilibrium simulation (EQ1), calcite initially present in the column was completely removed by pore volume two. Although Stollenwerk (1994) assumed that carbonate minerals were completely dissolved as the measured pH decreased to less than 4 by the end of pore volume two, it is possible that less reactive forms of carbonate, such as dolomite, or coated calcite, could have remained in the column through the length of the experiment. Simulated pH values from EQ1 decreased to about 4.5 by pore volume 3 and to about 4 by pore volume 8 (Fig. 4). In simulation CK1, all the calcite initially present in the column was depleted by pore volume 5.6. In the absence of calcite in the simulated column, it was expected that simulated pH would invariably decrease to less than 4. The pH, however, remained above 4 for pore volumes 5–9. No single cause for this higher-than-expected pH was readily apparent, but decreasing the calcite dissolution rate affected the concentration and speciation of several constituents, as well as the speciation of surface sites and the pH dependent equilibrium precipitation of Fe hydroxide.

Table 8
Dissolution and precipitation processes in column simulations

Simulation	Calcite	Dolomite	Mn oxide	Rate expression
EQ1	Equilibrium	–[a]	Equilibrium	–[b]
EQ2	Equilibrium	Equilibrium	Equilibrium	–[b]
CK1	Kinetic	–[a]	Equilibrium	Plummer et al. (1978) lab rate
CK2	Kinetic	–[a]	Equilbrium	Plummer et al. (1978) lab rate $\times 10^{-3}$
DK1	Equilibrium	Kinetic	Equilibirum	Busenberg and Plummer (1982) lab rate
DK2	Equilibrium	Kinetic	Equilibrium	Busenberg and Plummer (1982) lab rate $\times 10^{-3}$
PK	Equilibrium	–[a]	Kinetic	Column-fitted rate (this paper)

[a] Mineral not included in simulation.
[b] No kinetics in simulation.

The net result was an unrealistically high pH in column outflow from pore volume 2 through the end of the simulation.

In simulation CK2, which incorporated the approximate in situ calcite dissolution rate, calcite dissolution was insignificant in the column. The simulated acidic breakthrough occurred about 1 pore volume before the measured breakthrough, which occurred at pore volume 3. In the absence of significant calcite dissolution, the breakthrough of protons was controlled by the acidity of column inflow, the reductive dissolution of Mn oxide, and oxidation and precipitation of Fe hydroxide. The net reaction creates 2 protons for each mole of Mn oxide dissolved.

Neither of the kinetic simulations improved upon the equilibrium model, at least as far as calcite dissolution was concerned. Because the local equilibrium assumption for calcite appeared to be valid for conditions in the column, subsequent column simulations that incorporated dolomite or Mn kinetics were done without including calcite kinetics.

4.2. Dolomite

In order to assess the effects of dolomite dissolution kinetics, dolomite was added to simulation EQ1. The initial dolomite concentration for this simulation (EQ2) was set to 0.0067 mol/l_{water} on the basis of a mass balance done by Stollenwerk (1994) on Mg in column outflow. The initial calcite concentration of 0.067 mol/l_{water} was decreased by this amount. Despite the fact that the simulated dolomite and calcite were completely consumed by pore volume 2.5, the pH of column outflow for EQ2 remained greater than 4.5 until about pore volume 10, more than 2 pore volumes later than in simulation EQ1. This difference stemmed mainly from the fact that in EQ2, simulated dolomite and Mn oxide were completely dissolved from the column at the same time, whereas in EQ1, simulated calcite was completely dissolved just before MnO_2. In the absence of any neutralizing capacity, protons generated by MnO_2 dissolution dropped the pH in EQ1 to less than 3.5 in the downward spike at pore volume 2.5 (Fig. 4). As a result, the proton concentration at surface sites in EQ1 was from that point on larger than the concentration in EQ2 and reached a maximum at about pore volume 7, at which time the simulated pH decreased to less than 4. In EQ2, the concentration of protons at adsorption sites increased until pore volume 9.5, at which time simulated pH decreased to less than 4.

For DK1, dolomite dissolution kinetics were simulated using the rate expression [Eq. (2)] developed by Busenberg and Plummer (1982). This rate was lowered by 3 orders of magnitude in simulation DK2 to represent the rate estimate derived from the dolomite in situ experiments. DK1 and DK2 used a PARM1 value of 228, which was based on the initial dolomite concentration in the simulated column. Both simulations exhibited a downward spike in pH between pore volumes 2 and 3, during which time pyrolusite dissolution continued in the absence of calcite in the simulated column. In both simulations, pyrolusite was completely consumed by pore volume 2.5. In simulation DK1, pH then increased to more than 5 and remained greater than 5 for the remainder of the simulation. The lower dolomite dissolution rate used in simulation DK2 resulted in a better fit of simulated and measured pH for the remainder of the column experiment; however, only 2% of the dolomite initially in the simulated column dissolved over the course of the simulated column experiment. This amount was much less than that indicated by a mass balance on the outflow of dissolved Mg from the column. Because of this mass-balance discrepancy, the authors feel simulation DK2 to be unreasonable despite the improved match of measured and simulated outflow pH.

4.3. Manganese oxide

Mn oxide dissolution kinetics were simulated using a rate expression developed by Postma and Appelo (2000) and incorporated into PHREEQC by Parkhurst and Appelo (1999). In this expression, the dissolution rate is a function of pH and of the dissolved Fe concentration:

$$R = k' \times \left[Fe^{2+}\right] \times (m/m_0)^n \times (1 - IAP/K_{birn}) \quad (5)$$

where R is the birnessite dissolution rate in mol/(l s), and k' mol/(l s), is the apparent rate constant where $k' = kA_0/V$, with k being the rate constant in mol/(cm^2 s), and A_0/V being the initial surface area of the mineral per liter pore volume in cm^2/l_{pv}, $[Fe^{2+}]$ is the activity of Fe^{2+} in solution (unitless), m_0 and m are the initial and remaining masses of mineral in mol/l_{pv}, IAP is the ion activity product for birnessite, and K_{birn} is the solubility product constant for birnessite. The term $(m/m_0)^n$ describes the change in dissolution rate during bulk mineral dissolution. Using a trial-and-error fitting procedure, Postma and Appelo (2000) obtained a reasonable fit of their experimental data with a k' value of 6.98×10^{-5} mol/(l s) (Table 10) and an n value of 0.67. They noted, however, that different combinations of k' values and reaction orders (with respect to $[Fe^{2+}]$) produced identical results.

The Mn oxide concentration in uncontaminated alluvium was estimated to be 0.045 mol/l_{water} on the basis of sequential extraction (Stollenwerk, 1994). Although the exact form of Mn oxide in the alluvium was not determined, the rate expression for birnessite was used as a starting point in part because of the lack of pyrolusite dissolution measured during the in situ experiment. This was the initial simulated concentration of Mn oxide used in the column simulation. The chemical behavior

Table 9
Manganese oxide dissolution processes in field simulations

Simulation	Acidic zone	Neutralized zone
FLD1	–[a]	Equilibrium
FLD2	Kinetic[b]	Kinetic[b]
FLD3	Kinetic[c]	Kinetic[c]

[a] Mn oxide absent in acidic zone.
[b] Column-fitted rate.
[c] Field-fitted rate.

Table 10
Measured and model-fitted estimates of birnessite rate constants for expression of Postma and Appelo (2000)

Rate constant adjustment	Rate constant (mol/l s)
k' unadjusted	6.98×10^{-5}
k' fitted to column simulation	2.50×10^{-6}
k' fitted to field simulation	6.98×10^{-9}

of Mn in the column and in the plume was complicated by the fact that the concentration of dissolved Mn was controlled not only by the reductive dissolution of Mn oxide but also by the pH-dependent adsorption and desorption of dissolved Mn to and from Fe-hydroxide solids. The concentration of dissolved Ni in column outflow evidently was controlled solely by pH-dependent surface reactions (Stollenwerk, 1994) and was used to constrain the concentrations of surface sites. The surface complexation behavior of Mn, Ni, and selected other species (Table 7) is determined through the use of mass-action equations and associated intrinsic complexation constants, which generally are derived from solutions containing a single sorbate. The uncertainty of applying these constants in real solutions that contain multiple, potentially competing sorbate species is a significant source of uncertainty to this and similar analyses.

The simulated Ni and Mn breakthrough curves (Figs. 6 and 7) were fitted to measured breakthrough curves through an iterative procedure in which the Mn oxide dissolution rate and the concentration of surface-sites was adjusted individually. The best fit of measured and simulated breakthrough for Ni and Mn was achieved using a surface-site density of 0.972 mol/l for strong sites and 38.9 mol/l for weak binding sites. These site densities were 20% of the values used for HFO by Dzombak and Morel (1990).

The Mn oxide dissolution rate constant of 2.5×10^{-6} used to fit the model was less than the value of 6.98×10^{-5} obtained by Postma and Appelo (2000; Table 10). Incorporating Mn oxide kinetics and adjusting the number of surface sites in the model delayed the simulated decline to a pH of less than 4 by about 1 pore volume, but matched the measured pH better than the equilibrium model from pore volumes 4–7 (Fig. 8). The simulated equilibrium and kinetic pH values were virtually identical for pore volumes 8–20. Mass–balance calculations of measured Mn inflow to and outflow from the column indicate that approximately 0.015 mol/l_{water} of Mn oxide in the column dissolved over the course of the experiment, although the sequential chemical extraction done on the reacted alluvium yielded a decrease of 0.031 mmol/l_{water} (Stollenwerk, 1994).

In the equilibrium and kinetic simulations, the Mn oxide initially in the column was completely consumed by pore volumes 2.6. and 8.6, respectively. The good match between the magnitude of the measured and simulated kinetic Mn breakthrough peaks (Fig. 9) suggests that the chosen rate constant is applicable to at least some of the Mn oxide in the column, but the persistence of Mn oxide in the actual column following the passage of almost 11 pore volumes of acidic water

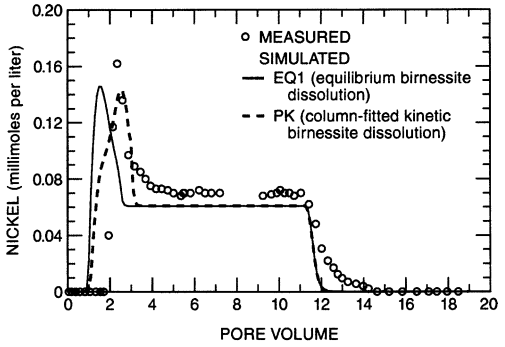

Fig. 6. Measured and simulated concentrations of dissolved Ni in column effluent showing the effect of equilibrium and kinetic birnessite dissolution. Kinetic birnessite rate equation from Postma and Appelo (2000). Column simulation parameters are summarized in Tables 5–8.

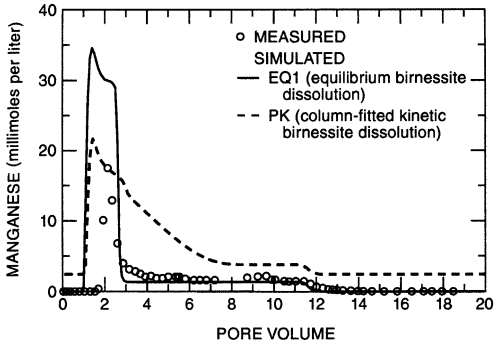

Fig. 7. Measured and simulated concentrations of dissolved Mn in column effluent showing the effect of equilibrium and kinetic birnessite dissolution. Kinetic birnessite rate equation from Postma and Appelo (2000). Column simulation parameters are summarized in Tables 5–8.

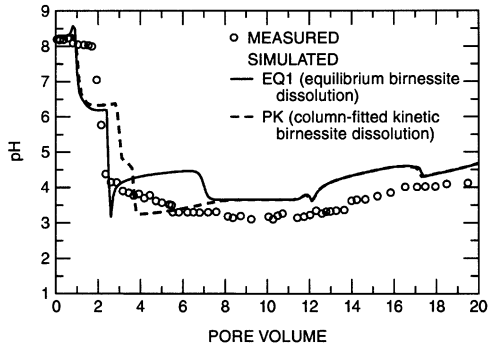

Fig. 8. Measured and simulated pH in column effluent showing the effect of equilibrium and kinetic birnessite dissolution. Kinetic birnessite rate equation from Postma and Appelo (2000). Column simulation parameters are summarized in Tables 5–8.

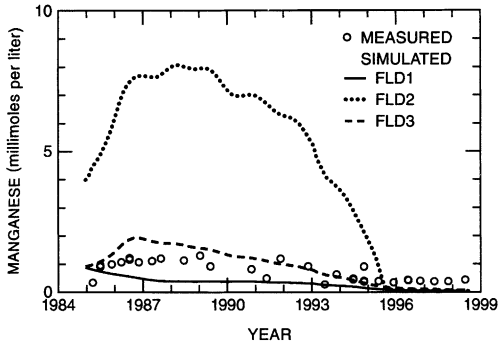

Fig. 9. Measured and simulated concentrations of dissolved Mn in water in the acidic zone from well 402, 1984–1998. Simulation FLD1: birnessite absent in acidic zone; FLD2: column-fitted kinetic birnessite dissolution rate; FLD3: field-fitted birnessite dissolution rate. Field simulation parameters are summarized in Tables 1, 6, 7, 9, and 10.

suggests that the remaining Mn oxide was relatively less reactive than the Mn oxide that dissolved. Sequential chemical extractions indicated that some of the Mn was associated with amorphous Fe (Stollenwerk, 1994); perhaps this Mn oxide was less reactive than other form(s) initially in the column. Mn oxides initially in the column could also have become coated with Fe or gypsum precipitates during the experiment and rendered less reactive as a result. Another possibility, initially raised by Stollenwerk (1994), was that some of the Mn that dissolved may have subsequently co-precipitated with Fe hydroxides. Co-precipitation was not simulated because of the lack of thermodynamic information on mixed Fe–Mn hydroxides.

5. Kinetic geochemical transport modeling at the field scale

In order to assess the effect of rate-limited Mn oxide dissolution at the field scale, Mn oxide reaction kinetics were incorporated into an existing one-dimensional equilibrium reactive transport model of the plume at Pinal Creek (Brown et al., 1998). This model simulated plume evolution along a 16-km-long flow path from well 51 to well 702 (Fig. 1) from 1984 to 1994. The flow path was represented by 82 cells, each 200 m in length. The average estimated ground-water flow velocity of 5 m/d was simulated in the model by using a time step of 40 days. The dispersivity value used was 30 m. Brown et al. (1998) found that varying the dispersivity from 0 to 60 m had little discernable effect on the evolution of the plume for 1984–1994. Similarly, in a smaller-scale (5.6 km) 1-dimensional simulation Glynn and Brown (1996) found that varying the dispersivity between 0 and 560 m did not significantly affect the transport of reactive constituents.

The measured water chemistry from monitor well 51 (Table 1) provided the inflow chemistry to the 16-km model. Well 51 was the USGS monitor well closest to the upgradient sources of contamination. Reactive phases specified were calcite, dolomite, gypsum, ferrihydrite [$Fe(OH)_{3(a)}$], Mn oxide, and rhodochrosite (Table 6). For this analysis, two significant changes were made to the Brown et al. (1998) model: (1) the simulation period was extended to June 1998 and (2) the surface site concentration was increased by a factor of 4 to the fitted concentration used in the column simulation discussed earlier. The equilibrium reactions used in the present simulation and in the 1998 simulation are otherwise identical, except for minor changes in model input required to convert the 1998 model to version 2 of PHREEQC. The present analysis focuses on the Mn oxide dissolution rate and on the related geochemical evolution of the contaminant plume. Brown et al. (1998) offer a more complete analysis of the observed and simulated evolution of the contaminant plume (Fig. 2) at the Pinal Creek site.

For the 3 field simulations done for this analysis (Table 9), the initial Mn oxide concentration in the neutralized zone was set to 0.045 mol/l_{water}. Simulation FLD1 was identical to the equilibrium simulation of Brown et al. (1998) except for the changes mentioned above. This simulation allowed for equilibrium dissolution of Mn oxide in the transition and neutralized zones (from km 9 to km 16 in 1984) and no Mn oxide dissolution in the acidic zone. Simulations FLD2 and FLD3 allowed for rate-limited Mn oxide dissolution from km 3 to the end of the simulated flow path (Table 9).

In the transition zone, equilibrium Mn oxide dissolution and desorption generated a dissolved Mn peak of 13 mmol/l at km 10 in 1991 (Fig. 10). The highest concentration measured in or near the transition or

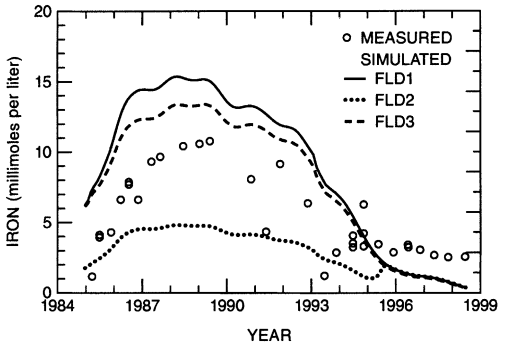

Fig. 10. Measured and simulated concentrations of dissolved Fe in water in the acidic zone from well 402, 1984–1998. Simulation FLD1: birnessite absent in acidic zone; FLD2: column-fitted kinetic birnessite dissolution rate; FLD3: field-fitted birnessite dissolution rate. Field simulation parameters are summarized in Tables 1, 6, 7, 9, and 10.

neutralized zones was 2.7 mmol/l at monitor well LE1 in 1989 (Hydro Geo Chem, 1989). Simulation FLD2, which used the column-fitted k' of 2.50×10^{-6} mol/(l s), caused the peak to decrease only slightly, to 12 mmol/l (not shown). Decreasing k' to 6.98×10^{-9} mol/(l s) for simulation FLD3 lowered the simulated 1991 Mn peak to 6.2 mmol/l (Fig. 11). The remaining differences may relate only in part to reaction rate. It is possible that larger Mn concentrations were present in the plume in zones not penetrated by wells. Although this analysis cannot determine with certainty the exact field dissolution rate, it is evident that the field rate is significantly lower than either the column-derived k' of 2.50×10^{-6} mol/(l s), or the k' of 6.98×10^{-5} mol/(l s) obtained by Postma and Appelo (2000).

In the acidic zone, Mn oxide concentrations in simulation FLD1 (the equilibrium simulation) were set to zero because sequential extractions done by Ficklin et al. (1991) indicated that Mn oxide in the acidic part of the plume was largely depleted. Brown et al. (1998) assumed that any Mn oxide persisting in the aquifer after acidification would be less reactive than the Mn that dissolved, and that Mn reactions in the acidic zone would be insignificant. However, for FLD1, simulated concentrations of dissolved Mn were lower than measured concentrations, and simulated concentrations of dissolved Fe were higher than measured concentrations (Figs. 9 and 12). These differences, at least in part, were attributed by Brown et al. (1998) to the continued (and nonequilibrium) reductive dissolution of Mn oxide coupled to the oxidation and precipitation of Fe hydroxide in the acidic zone. To assess the effect of rate-limited Mn oxide dissolution in the acidic zone, kinetic dissolution in the acidic zone was allowed for in simulations FLD2 and FLD3, with an initial Mn oxide concentration of 0.008 mol/l_{water} from km 3 to km 9.

As mentioned previously, simulation FLD2 used the column-calibrated k' of 2.50×10^{-6} mol/(l s) (Table 10). This produced unreasonably high simulated concentrations of dissolved Mn in water at well 402. The maximum measured and simulated dissolved Mn concentrations in water from well 402 were 8 and 2 mmol/l, respectively (Fig. 9). A closer fit was obtained by decreasing k' to 6.98×10^{-9} mol/(l s) (Table 10) in simulation FLD3. Further adjustments of the rate likely would have improved the Mn fit, but would also have increased the difference between the simulated and measured Fe concentrations at well 402 (Fig. 12).

As expected, the way in which Mn oxide dissolution was simulated affected simulated pH values along the flow path and the rate of movement of the pH front. For FLD1, simulated pH in the acidic zone (in the absence of Mn dissolution) increased from less than 4 in 1984 to as much as 5 by 1998 (Fig. 13). Incorporating Mn oxide kinetic dissolution with a k' of 6.98×10^{-9}

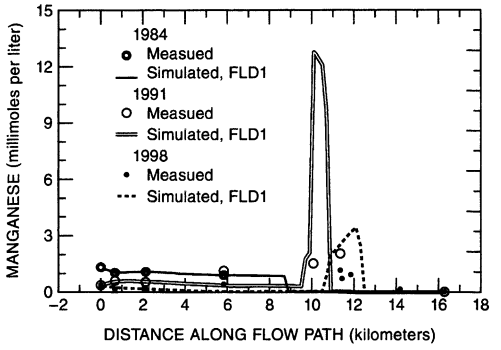

Fig. 11. Measured and simulated concentrations of dissolved Mn along the flow path, 1984, 1991, and 1998. Simulation FLD1: equilibrium birnessite dissolution in the transition and neutralized zones; birnessite absent in acidic zone. Field simulation parameters are summarized in Tables 1, 6, 7, 9, and 10.

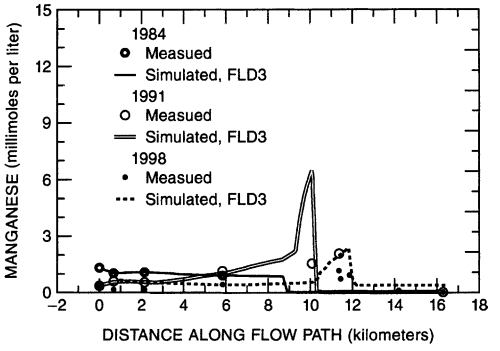

Fig. 12. Measured and simulated concentrations of dissolved Mn along the flow path, 1984, 1991, and 1998. Simulation FLD3: field-fitted kinetic birnessite dissolution rate from km 3 to end of flowpath. Field simulation parameters are summarized in Tables 1, 6, 7, 9, and 10.

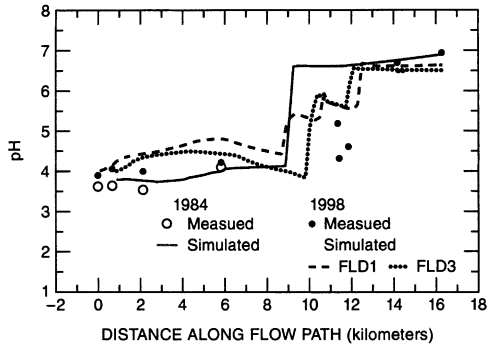

Fig. 13. Measured and simulated pH along the flow path, 1984 and 1998. Simulation FLD1: equilibrium birnessite dissolution in the transition and neutralized zones; birnessite absent in acidic zone; FLD3: field-fitted kinetic birnessite dissolution rate from km 3 to end of flowpath. Field simulation parameters are summarized in Tables 1, 6, 7, 9, and 10.

mol/(l s) lowered the 1998 simulated pH from km 4 to km 9 by as much as one-half unit, into better agreement with the measured pH at km 6.

In the equilibrium simulation, the Mn oxide initially present from km 8 to km 10.1 was completely consumed, and the pH in that interval decreased from 6.7 to about 5.3. Allowing for kinetic dissolution of Mn oxide in both the acidic and transition zones decreased the simulated pH values to less than 4 between km 8 and km 10.1. In both simulations, however, pH values were unreasonably high between km 11 and km 12 (Fig. 11). The remaining differences between measured and simulated chemistry are likely related, at least in part, to factors other than the Mn dissolution rate. Those factors might include the concentration of surface sites available for adsorption, the effects of competition among dissolved species for available surface sites, or reactions not included in the model. For example, reactions involving Al-containing minerals [such as amorphous $Al(OH)_3$, gibbsite, jurbanite, or kaolinite] were not included in the model. These reactions can be expected to have significant and differing impacts on the distribution and evolution of pH values, as demonstrated in the reaction sensitivity analysis conducted by Glynn and Brown (1996) for a small-scale (5.6 km) field simulation of the Pinal Creek site. Physical factors that could contribute to differences between simulated and measured chemistry include lithologic heterogeneities, or changing ground-water levels that could alter the flow path between wells in the simulation.

6. Summary and conclusions

The kinetics of calcite, dolomite, and pyrolusite dissolution were examined through the in situ exposure of pure-phase samples to acidic, reducing ground water for periods of time ranging from 14 to 595 days. Results from the in situ experiment were compared with results of laboratory rates derived by other investigators, and the application of the in situ and lab-derived rates to real systems was examined by the incorporation of these rates into numerical models of dissolution at the column and field scales. Modeled rates were adjusted where necessary to better fit the geochemical evolution of acidic water and dissolved Mn concentrations observed in a column experiment (Stollenwerk, 1994) and at the Pinal Creek field site.

The calculated average long-term in situ dissolution rates were 1.65×10^{-9} mmol/(cm^2 s) for calcite and 3.64×10^{-10} mmol/(cm^2 s) for dolomite, about 3 orders of magnitude slower than rates derived in laboratory experiments done by Plummer et al. (1978) and Busenberg and Plummer (1982), respectively. Application of calcite and dolomite kinetic dissolution to an equilibrium reactive-transport simulation of a column experiment did not improve the fit of measured and simulated outflow chemistry. At the spatial and temporal scales of the column experiment, the use of an equilibrium model was adequate to simulate carbonate dissolution in the column.

Mn oxide samples exposed to acidic water in well 101 for 241 and 570 days increased in weight slightly during the in situ experiment despite thermodynamic conditions that favored dissolution. Villinski et al. (2001) found that the dissolution of MnO_2 under similar conditions in a laboratory flow-through cell was accompanied by the precipitation of a phase with the structure of jacobsite ($MnFe_2O_4$). The formation of this phase could at least partially explain the weight increases measured during the in situ experiment. Another reason might be related to the uncertainty of the actual Mn oxide phase present in the aquifer. In addition, the use of birnessite or some other Mn oxide mineral, rather than pyrolusite, might have produced different results.

Mn breakthrough in a column experiment was matched by reducing k' in the rate equation for birnessite dissolution developed by Postma and Appelo (2000) from 6.98×10^{-5} mol/(l s) to 2.50×10^{-6} mol/(l s). Neither k' was evidently applicable to the field situation. The former k' was reduced by 4 orders of magnitude to better fit the distribution and evolution of dissolved Mn and Fe concentrations in the transition zone and in the acidic part of the plume (at well 402) through 1992. Kinetic Mn oxide dissolution decreased the unreasonably large Mn peak in the transition zone, but the simulated pH remained about 1 unit higher than the observed pH. Remaining differences between simulated and measured ground-water chemistry were most likely related to factors other than the rate of Mn oxide dissolution, such as the concentration of Fe oxide surface sites available for adsorption, the effects of competition among dissolved species for available surface sites, or reactions not included in the model. Rate constants

developed from the batch and column experiments discussed in this paper are likely not applicable to reactions that are occurring in the aquifer in Pinal Creek Basin.

Acknowledgements

The authors would like to thank Cory Angeroth of the USGS for field support, and David Parkhurst of the USGS for assistance with PHREEQC. This work was funded by the USGS Toxic Substances Hydrology Program.

References

Brown, J.G., Bassett, R.L., Glynn, P.D., 1998. Analysis and simulation of reactive transport of metal contaminants in ground water in Pinal Creek Basin, Arizona. J. Hydrol. 209, 225–250.

Brown, J.G., Bassett, R.L., Glynn, P.D., 2000. Reactive transport of metal contaminants in alluvium—model comparison and column simulation. Appl. Geochem. 15, 35–50.

Brown, J.G., Favor, B. (Eds.), 1996. Hydrology and Geochemistry of Aquifer and Stream Contamination Related to Acidic Water in Pinal Creek Basin near Globe. Arizona. US Geol. Surv. Water-Supply Pap. 2466.

Busenberg, E., Plummer, L.N., 1982. The kinetics of dissolution of dolomite in CO_2-water systems at 1.5° to 65 °C and 0.0 to 1.0 atmosphere P_{CO_2}. Am. J. Sci. 282, 45–78.

Dzombak, D.A., Morel, F.M.M., 1990. Surface Complexation Modeling—Hydrous Ferric Oxide. Wiley-Interscience, New York.

Eychaner, J.H., 1991. The Globe, Arizona, research site—contaminants related to copper mining in a hydrologically integrated environment. In: Mallard, G.E., Aronson, D.A. (Eds.), US Geological Survey Toxics Substance Hydrology Program—Proc. Technical Meeting, Monterey, CA, 11–15 March 1991. US Geol. Surv. Water-Resour. Invest. Rep. 91-4034, pp. 439–447.

Ficklin, W.H., Love, A.H., Briggs, P.K., 1991. Analytical Results for Total and Partial Metal Extractions in Aquifer Material, Pinal Creek, Globe, Arizona. US Geol. Surv. Open-File Rep. 91-111.

Glynn, P.D., Brown, J.G., 1996. Reactive transport modeling of acidic metal-contaminated ground water at a site with sparse spatial information. In: Steefel, C.I., Lichtner, P., Oelkers, E. (Eds.), Reactive Transport in Porous Media: General Principles and Application to Geochemical Processes. Mineralogical Society of America, Reviews in Mineralogy, 34, 377–438.

Hydro Geo Chem, 1989. Investigation of Acid Water Contamination along Miami Wash and Pinal Creek, Gila County, Arizona. Claypool, Arizona Cyprus Miami Mining Corporation, Claypool, AZ.

Lind, C.J., Creasey, C.L., Angeroth, C., 1998. In situ alteration of minerals by acidic ground water resulting from mining activities: preliminary evaluation of method. J. Geochem. Explor. 64, 293–305.

Morganwalp, D.W., Buxton, H.T. (Eds.), 1999. US Geological Survey Toxic Substances Hydrology Program—Proc. Technical Meeting, Charleston, SC, 8–12 March 1999, Vol. 1 of 3, Contamination from Hardrock Mining. US Geol. Surv. Water-Resour. Invest. Rep. 99-4018A, pp. 139–258.

Neaville, C.C., Brown, J.G., 1994. Hydrogeology and Hydrologic System of Pinal Creek Basin, Gila Country, Arizona. US Geol. Surv. Water-Resour. Invest. Rep. 93-4212.

Parkhurst, D.L., 1995. User's Guide to PHREEQC—A Computer Program for Speciation, Reaction-path, Advective-transport, and Inverse Geochemical Calculations. US Geol. Surv. Water-Resour. Invest. Rep. 95-4227.

Parkhurst, D.L., Appelo, C.A.J., 1999. User's Guide to PHREEQC (Version 2)—A Computer Program for Speciation, Batch-reaction, One-dimensional Transport, and Inverse Geochemical Calculations. US Geol. Surv. Water-Resour. Invest. Rep. 99-4259.

Plummer, L.N., Wigley, T.M.L., Parkhurst, D.L., 1978. The kinetics of calcite dissolution in CO_2-water systems at 5° to 60 °C and 0.0 to 1.0 atm CO_2. Am. J. Sci. 278, 179–216.

Postma, D., Appelo, C.A.J., 2000. Reduction of Mn oxides by ferrous iron in a flow system: column experiment and reactive transport modeling. Geochim. Cosmchim. Acta 64, 1237–1247.

Stollenwerk, K.G., 1994. Geochemical interactions between constituents in acidic groundwater and alluvium in an aquifer near Globe, Arizona. Appl. Geochem. 9, 353–369.

Villinski, J.E., O'Day, P.A., Corley, T.L., Conklin, M.H., 2001. In situ spectroscopic and solution analyses of the reductive dissolution of Mn02 by Fe(II). Environ. Sci. Technol. 35, 1157–1163.